

Electronic Supplementary Information†

Transformation of a proton insulator to a conductor *via* reversible amorphous to crystalline structure transformation of MOFs

Yoodae Song,^{a,b} Alexander E. Khudozhitkov,^{c,d} Jihyun Lee,^b Hyosik Kang,^b Daniil I.
Kolokolov,^{c,d*} Alexander G. Stepanov,^{c,d} Minyoung Yoon^{a*}

^a*Department of Chemistry, Kyungpook University, Daegu 41566, Republic of Korea*

^b*Department of Nanochemistry, Gachon University, Seongnam 13420, Republic of Korea*

^c*Boreskov Institute of Catalysis, Siberian Branch of Russian Academy of Science, Novosibirsk
630090, Russia*

^d*Novosibirsk State University, Novosibirsk 630090, Russia*

*Corresponding author.

E-mail address: myyoon@knu.ac.kr (M. Yoon) kdi@catalysis.ru (D. I. Kolokolov)

1. Preparation of Metal-Formate

1.1 Materials

All the metal salts and ligands were purchased from Sigma Aldrich. All organic solvents were purchased from a local Korean company, Samchun Chemical, Gyeonggi-Do, South Korea. All chemicals were used as received without further purification.

1.2 Preparation of Mg(HCO₂)₂

A solution of magnesium perchlorate hexahydrate (0.662 g, 2.00 mmol) and formic acid (0.184 mg, 4.00 mmol) in N, N-diethylformamide (8.0 mL) and 1, 4-dioxane (4.0 mL) was divided into 4 sealed glass tubes. The sealed glass tubes were heated to 120 °C in a convection oven. After 48 hours, white crystals were collected by filtration and washed with fresh DMF and methylene chloride (10 mL x 3 times). The crystals were then dried at 130 °C under dynamic vacuum to remove the template molecules (1, 4-dioxane) resulting in the phase I material.^{S1}

1.3 Preparation of Co(HCO₂)₂

A solution of cobalt perchlorate hexahydrate (0.731 g, 2.00 mmol) and formic acid (0.184 mg, 4.00 mmol) in N, N-dimethylformamide (8 ml) and 1, 4-Dioxane (4 ml) was prepared in a 20 ml vial. The 20 ml vial was heated at 110 °C in a convection oven. After 48 hours, pink crystals were collected by filtration and washed with fresh DMF and methylene chloride (10 mL x 3 times). The crystals were then dried at 130 °C under dynamic vacuum to remove template molecules (1,4-dioxane) resulting in the phase I material.

2. Characterization and Analysis

2.1 Single-crystal X-ray diffraction and structure analysis of phase I metal formate

Single crystals of solvent-free Mg(HCO₂)₂ and Co(HCO₂)₂ were coated with paratone-N oil. Diffraction data were recorded at 90 K for Mg(HCO₂)₂ and at 100 K for Co(HCO₂)₂ with

synchrotron radiation, using the ADSC Quantum 210 CCD detector with a silicon (111) double-crystal monochromator, from the 2D SMC beamline of the Pohang Accelerator Laboratory, Korea. The ADSC Q210 ADX software^{S2} was used for data collection (detector distance of 63 mm, omega scan; $\Delta\omega = 1^\circ$, and exposure times of 0.5 s per frame for $\text{Mg}(\text{HCO}_2)_2$ and 2 s per frame for $\text{Co}(\text{HCO}_2)_2$). The HKL3000sm (version 703r)^{S3} was used for cell refinement, reduction, and absorption correction. All crystal structures were solved by direct method and refined by full-matrix least-squares calculation using the SHELXS and SHELXL programs, respectively (version 2014).^{S4}

$\text{Mg}(\text{HCO}_2)_2$. Colorless block-shaped crystal, $0.035 \times 0.035 \times 0.014 \text{ mm}^3$, $\text{C}_6\text{H}_6\text{Mg}_3\text{O}_{12}$, FW = 343.04 g/mol, monoclinic, space group $P2_1/n$, $a = 11.350 (2) \text{ \AA}$, $b = 9.864 (2) \text{ \AA}$, $c = 14.566 (3) \text{ \AA}$, $\beta = 91.40 (3)^\circ$, $V = 1630.3 (6) \text{ \AA}^3$, $Z = 4$, $\mu(\lambda = 0.700 \text{ \AA}) = 0.222 \text{ mm}^{-1}$, 16,423 reflections collected of which 4,733 are unique ($R_{\text{int}} = 0.0294$). The positions of all non-H atoms were refined with anisotropic displacement factors. All H atoms were placed by using a riding model while their positions were constrained relative to their parent atoms using the appropriate HFIX command. Refinement of the structure converged at a final $R_1 = 0.0516$ and $wR2 = 0.1523$ for 3 898 reflections with $I > 2\sigma(I)$, $R_1 = 0.0601$, and $wR2 = 0.1575$ for all 4,733 reflections. The largest difference peak and hole were 0.794 and -0.584 e/\AA^3 , respectively.

$\text{Co}(\text{HCO}_2)_2$. Purple block-shaped crystal, $0.030 \times 0.030 \times 0.020 \text{ mm}^3$, $\text{C}_6\text{H}_6\text{Co}_3\text{O}_{12}$, FW = 446.90 g/mol, monoclinic, space group $P2_1/n$, $a = 11.269 (2) \text{ \AA}$, $b = 9.848 (2) \text{ \AA}$, $c = 14.466 (3) \text{ \AA}$, $\beta = 91.16 (3)^\circ$, $V = 1605.1 (6) \text{ \AA}^3$, $Z = 4$, $\mu(\lambda = 0.630 \text{ \AA}) = 2.220 \text{ mm}^{-1}$, 22,436 reflections collected of which 6,283 are unique ($R_{\text{int}} = 0.0560$). The positions of all non-H atoms were refined with anisotropic displacement factors. All H atoms were placed by using a riding model while their positions were constrained relative to their parent atoms using the appropriate HFIX command. Refinement of the structure converged at a final $R_1 = 0.0314$ and $wR2 = 0.0844$ for 5 471 reflections with $I > 2\sigma(I)$, $R_1 = 0.0368$, and $wR2 = 0.0869$ for all 6,283 reflections. The largest difference peak and hole were 0.623 and -1.479 e/\AA^3 , respectively.

The supplementary crystallographic data for this study can be found in CCDC-1945386 (Mg) and CCDC-1945385 (Co). The data can be obtained free of charge from www.ccdc.cam.ac.uk/conts/retrieving.html (or from the CCDC, 12 Union Road, Cambridge CB2

1EZ, UK; fax: +44 1223 336033; e-mail: support@ccdc.cam.ac.uk).

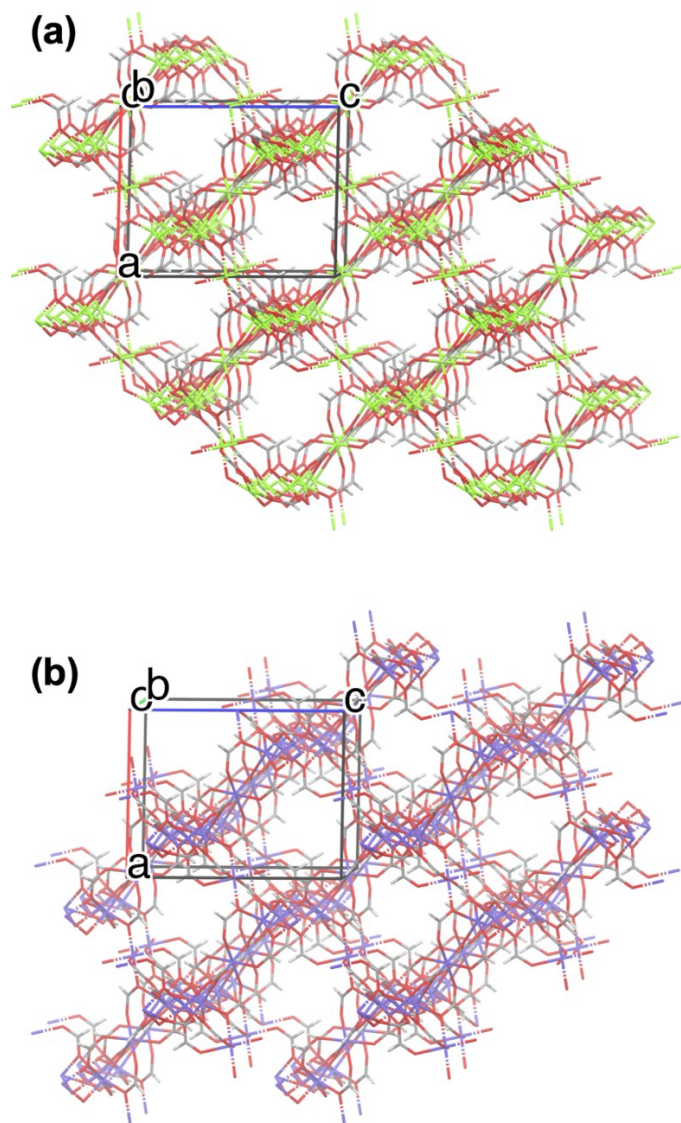


Fig. S1 Structures of (a) $\text{Mg}(\text{HCO}_2)_2$ and (b) $\text{Co}(\text{HCO}_2)_2$ phase I.

2.2 Unit cell parameter determination of phase III by indexing PXRD data

Home machine: The prepared metal-formates were analyzed using a Rigaku Ultima III X-ray diffractometer equipped with a Cu sealed tube ($\lambda = 1.54178 \text{ \AA}$). The following conditions were used: 40 kV, 30 mA, increment = 0.05° , scan speed = 3 deg/min.

Synchrotron: The samples were prepared by exposing the phase I materials to high RH at 25 °C for 6 hours using a temperature and humidity-controlled chamber (TH-ME-025, JEIOTECH). For the analysis of unit cell parameters of the DMOFs, diffraction patterns of the frameworks were measured using a synchrotron X-ray source (0.9000 Å) from the Pohang Accelerator Laboratory (2D SMC beamline), which was equipped with 2D area CCD detector. The framework sample was prepared in a 0.5 mm borosilicate capillary and mounted on a goniometer head. The diffraction data were collected using a Debye-Scherrer mode with a detector distance of 180 mm and an exposure time of 60 sec (720° rotation). The collected 2D diffraction image was merged and processed using a fit2d program.^{S5} The merged PXRD data was used for the determination of unit-cell parameters. First of all, we expect that the phase II it is expected that phase II is simply a structure where water is adsorbed in the pores of the MOFs. We succeeded in the separation of phase II in a pure form from Ni-formate, which confirmed that phase II is a water adsorbed structure. The PXRD data was indexed using Conograph GUI (developed by KEK and J-PARC neutron diffraction group, Japan).^{S6} For the characterization of phase III, the indexed parameter was selected based on the Wolff figure of merit and the unit cell parameter of the frameworks was subsequently determined. The refined diffraction data for Mg and Co are presented in Fig. S2 and 3. The calculated unit cell parameters are summarized in Table S1. The calculated unit cell parameters matched those of the reported $\text{Mg}(\text{HCO}_2)\cdot 2\text{H}_2\text{O}$ structure^{S7} found in the Cambridge Structural Database^{S8} and the $\text{Co}(\text{HCO}_2)\cdot 2\text{H}_2\text{O}$ reported by Kaufman and coworkers.^{S9}

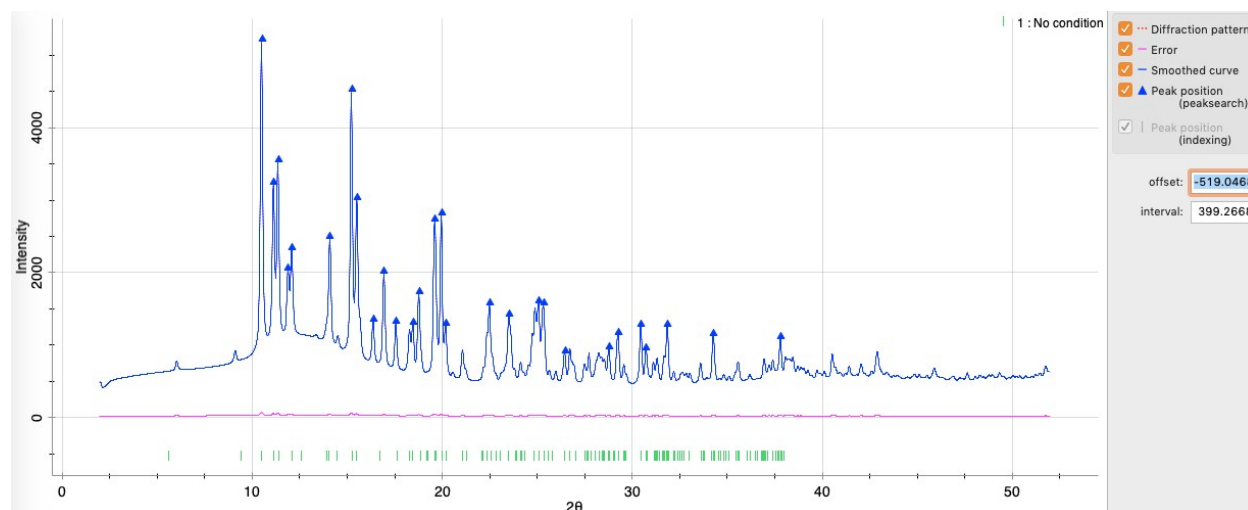


Fig. S2 PXRD indexed plot of $\text{Mg}(\text{HCO}_2)_2$ -phase III.

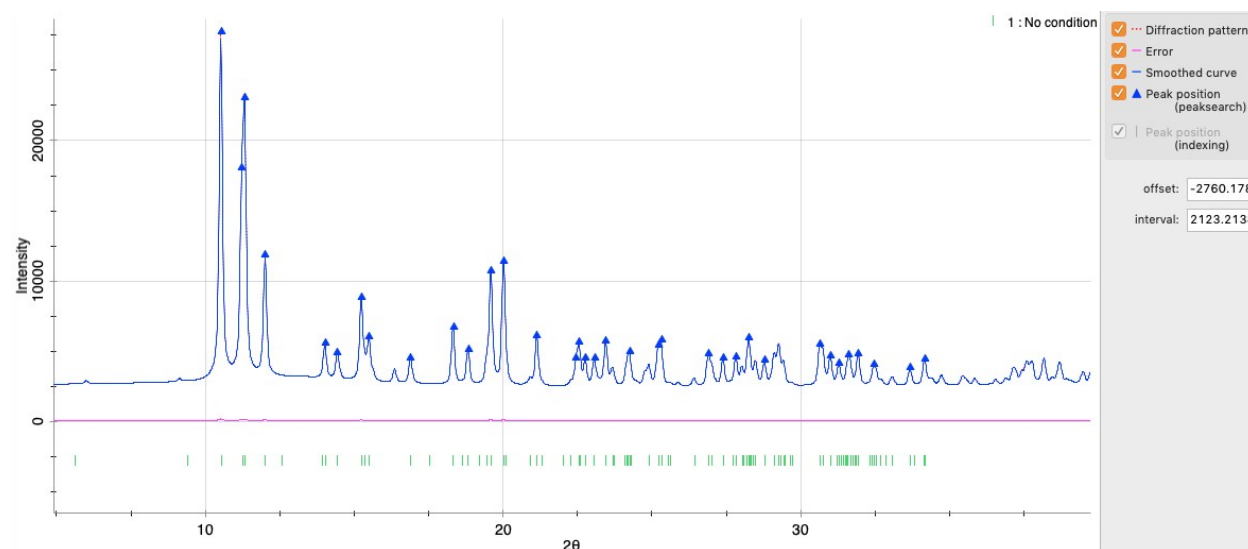


Fig. S3 PXRD indexed plot of $\text{Co}(\text{HCO}_2)_2$ -phase III.

Table S 1 Calculated unit cell parameters of the metal formate phase III

Sample	Suggested space group	$a(\text{Å})$	$b(\text{Å})$	$c(\text{Å})$	$\alpha=\gamma(^{\circ})$	$\beta(^{\circ})$
$\text{Mg}(\text{HCO}_2)_2$	5, 8, 12	8.65	7.20	9.39	90	98.1
$\text{Co}(\text{HCO}_2)_2$	5, 8, 12	8.68	7.17	9.29	90	97.5

Based on the reported structure,^{S7} the hydrogen bonding network in the crystal structure was analyzed (Fig. S4). There are two independent metal sites, one with four coordinated water molecules and the other without coordinated a water molecule. The magnesium metal ion with coordinated water molecules was aligned in a herringbone shape. The distance of water molecules in one metal center was 2.927 Å (O···O distance). In addition, two hydrogen bonding between two adjacent metal centers, which has 3.525 and 4.026 Å (O···O distances). Therefore, the 180 ° two sites flip motion, confirmed in ²H NMR experiment can explain the proton transport through the coordinated water molecules.

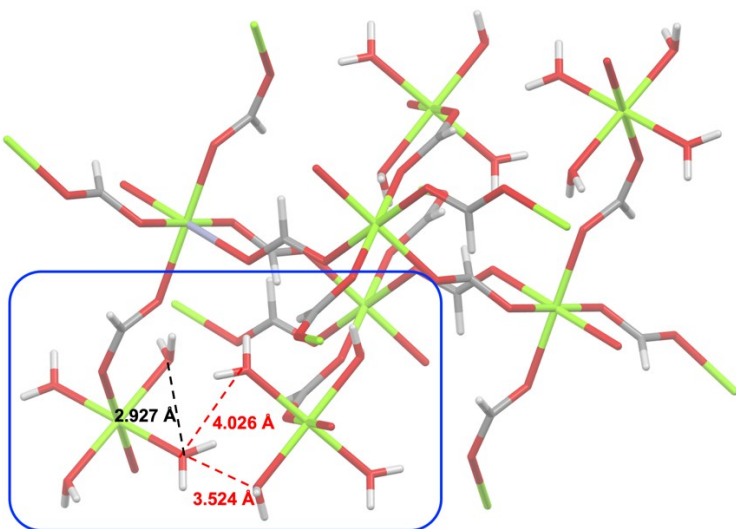


Fig. S4 Hydrogen bonding distances of the Mg(HCO₂)₂ phase III.

2.3 PXRD under various relative humidity conditions and recycling experiment

Preparation of phase I

The as-synthesized metal-formate was placed in CH₂Cl₂ for 2 days to exchange the solvent. The solvent exchanged MOF was dried at 130 °C under dynamic vacuum for a further 2 days. Because of the templating solvent, the MOF must be activated for at least 2 days otherwise the templating solvent (DMF or 1, 4-dioxane) will not be removed.

Preparation of phases II and III (mixture state)

MOF samples with a phase I structure (~100 mg) were placed in a 20 mL vial. The sample vial was placed in a temperature and humidity-controlled chamber at 60 % RH and 25 °C for 4 hours. The sample was recovered from the vial and used without further treatment.

Preparation of phase III (pure form)

MOF samples with a phase I structure (~100 mg) were placed in a 20 mL vial. The sample vial was placed in a temperature and humidity-controlled chamber at 95 % RH and 25 °C for at least 3 hours for $\text{Mg}(\text{HCO}_2)_2$ and 8 hours for $\text{Co}(\text{HCO}_2)_2$. The sample vial was sealed with a cap to prevent water evaporation before use.

Drying of amorphous structure (phase IV) and regeneration of hydrated structure (phase III)

Samples with a phase III structure were previously prepared by drying at 130 °C under dynamic vacuum. The dried MOF (phase IV) was placed in a 90 % RH humidity chamber for 30 min. This resulted in a crystalline material with a phase III structure.

2.4 Water vapor sorption analysis

The water vapor sorption-desorption isotherms of the MOFs were collected using ASAP-2020 (Micromeritics, USA). For the water vapor isotherm measurement, Millipore water was degassed by vacuum after the water vapor source was frozen three times. The P_0 of the water vapor at 25 °C was determined by the P_0 cell of the instrument. The vapor sorption isotherms were collected from 0 – 0.96 (22.86 mmHg) P/P_0 value (representing the 0 to 96 % RH). The sample temperature was kept constant during the measurement using an isothermal controller supplied by Protech Korea (Republic of Korea).

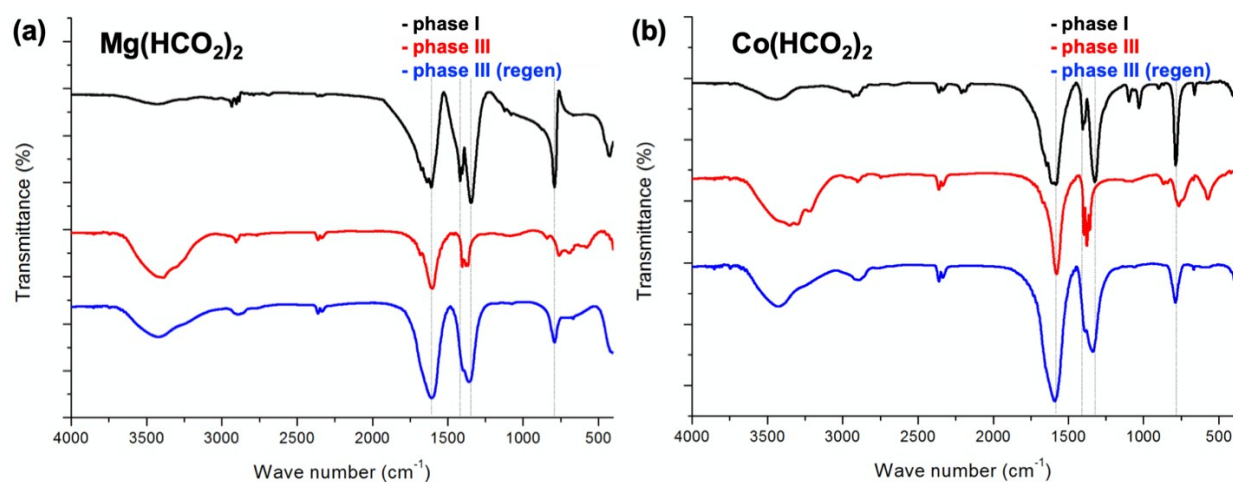


Fig. S5 FT-IR spectra of (a) $\text{Mg}(\text{HCO}_2)_2$ and (b) $\text{Co}(\text{HCO}_2)_2$ (black line: phase I, red line: phase III, and blue line: regenerated phase III from amorphous).

2.5 FT-IR experiment

The Fourier Transform-Infrared (FT-IR) spectra of both $\text{Mg}(\text{HCO}_2)_2$ and $\text{Co}(\text{HCO}_2)_2$ phase I and phase II were recorded by a Thermo iS-50 spectrometer in transmission mode (using a DTGD detector) with a 4 cm^{-1} resolution. The samples were ground with KBr and pressed into pellets (diameter: 0.7 cm, thickness: ~ 0.05 cm).

2.6 TGA experiments

The TGA data were collected using an N-1000 (SCINCO, Republic of Korea). An MOF sample (10 – 20 mg) was loaded into a platinum pan, which was placed in the furnace of TGA instrument. The sample containing pan was flushed with N_2 gas (600 mL/min) for an hour to produce an inert environment. The TGA data were collected using a ramping rate of $10^\circ/\text{min}$. We tried to calculate the amount of water molecules in the molecule. We concluded that the $\text{Mg}(\text{HCO}_2)_2$ contains 2.2 water molecules, and $\text{Co}(\text{HCO}_2)_2$ contains 2.3 water molecules. We can provide the molecular formula $[\text{Mg}(\text{HCO}_2)(\text{H}_2\text{O})_2] \cdot 0.2\text{H}_2\text{O}$ and $[\text{Co}(\text{HCO}_2)(\text{H}_2\text{O})_2] \cdot 0.3\text{H}_2\text{O}$ for Mg and Co, respectively. The TGA experiment supports the presence of unbound water molecules, which also participate in the proton conduction as proved in ^2H NMR experiment.

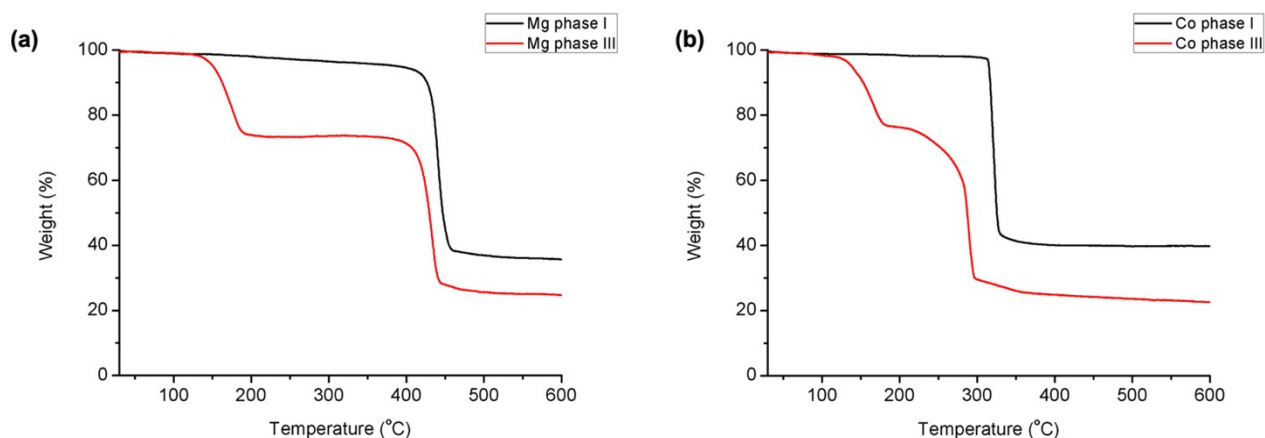


Fig. S6 TGA data of phase I and III for (a) $\text{Mg}(\text{HCO}_2)_2$ and (b) $\text{Co}(\text{HCO}_2)_2$

3. Impedance measurement for conductivity measurement

3.1 Impedance measurement under various relative humidity

The metal formate was ground and filled into a pelletizing cell with a diameter of 0.70 cm. The thickness of the pellet was ~ 0.06 cm, which was measured using a micrometer. Each side of the pellet was connected to a silver wire using silver paste. The pellet was placed in a temperature and humidity-controlled chamber (TH-ME-25, JEIOTECH) and exposed to the target temperature and humidity. The impedance was measured using a quasi-four probe method, in the 1– 100 MHz range, and a Bio-logic SP-200 with a high-resolution impedance probe.

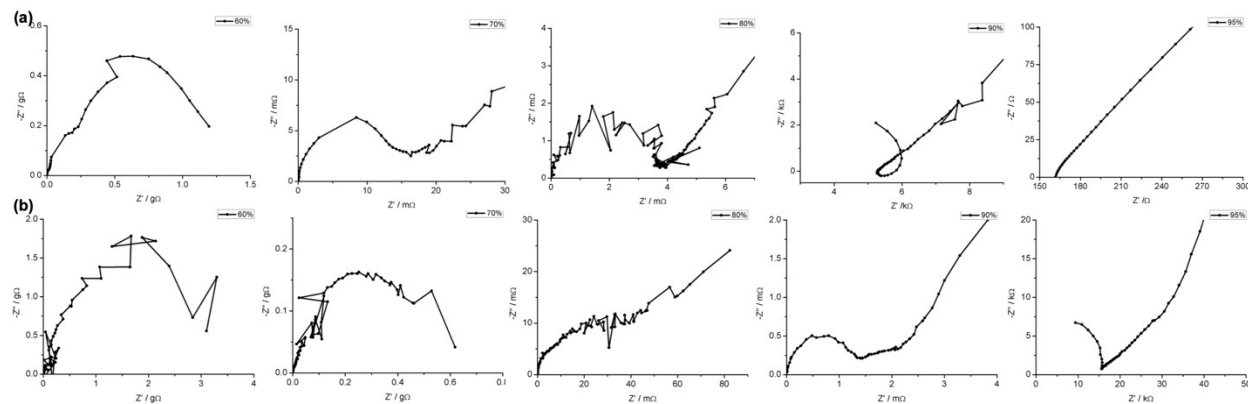


Fig. S7 Nyquist plots of (a) $\text{Mg}(\text{HCO}_2)_2$ and (b) $\text{Co}(\text{HCO}_2)_2$ at various relative humidity

3.2 Impedance measurement under various temperatures (for activation energy calculation)

To calculate the activation energy of phases II and III, the samples were placed under a fixed relative humidity (RH) while changing the temperature. For the $\text{Mg}(\text{HCO}_2)_2$ phase II, the RH was fixed at 60 % and the conductivity was measured from 25 – 45 °C with 5 °C increments. For the $\text{Co}(\text{HCO}_2)_2$ phase II, the RH was fixed at 70 % and the conductivity was measured from 25 – 45 °C with 5 °C increments. To calculate the activation energy of phase III, both samples were exposed to 95 % RH from 25 – 45 °C with 5 °C increments. The activation energy was calculated using the Arrhenius equation.

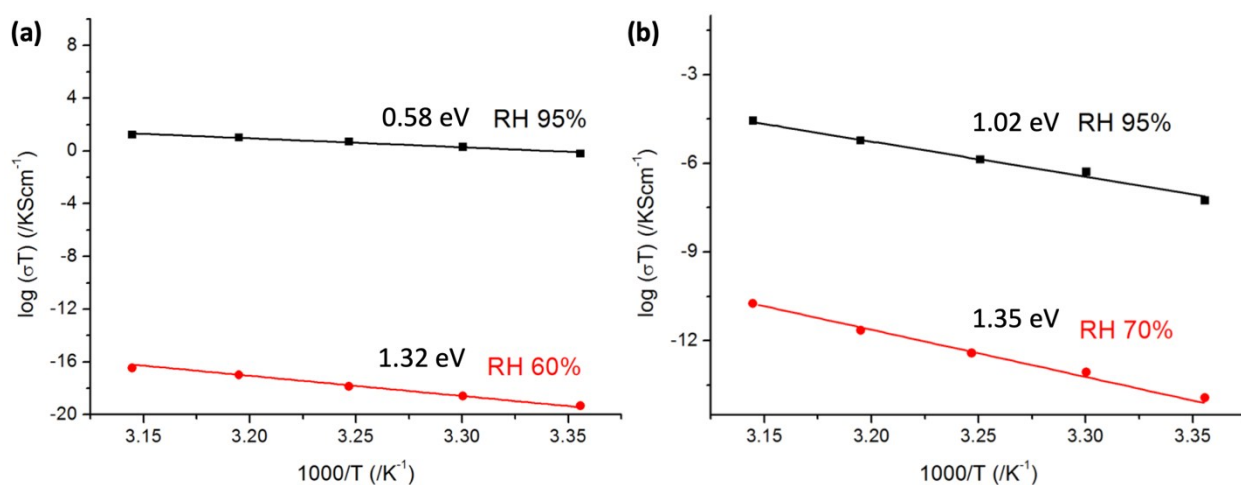


Fig. S8 Temperature dependent proton conductivity for activation energy calculation of (a) $\text{Mg}(\text{HCO}_2)_2$ and (b) $\text{Co}(\text{HCO}_2)_2$.

3.3 Impedance measurement for regenerated MOFs

The proton conductivity of the regenerated MOFs was also evaluated. The regenerated phase III sample was used for the proton conductivity measurements and it was analyzed under the same conditions of the original phase III sample. The conductivity values of the original and regenerated phase III are shown in Fig. S9 and although the conductivity of the regenerated phase was not exactly the same as that of the original phase, the values were in the same order of magnitude range.

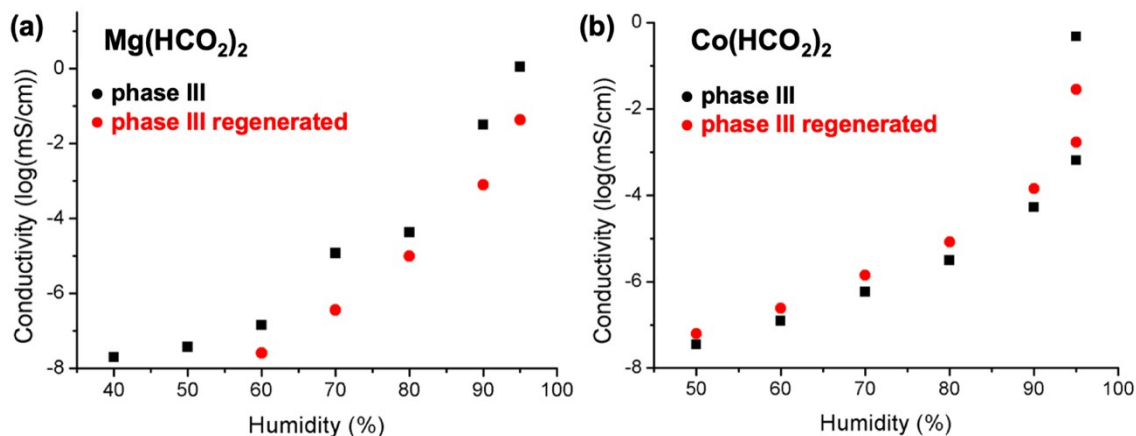


Fig. S9 Proton conductivity of both phase III and regenerated phase III of (a) Mg(HCO₂)₂ and (b) Co(HCO₂)₂

4. Solid-state ²H NMR experiment

4.1 Sample preparation

Only the Mg(HCO₂)₂ phase III was used for the NMR study because (1) bulk phase II was not separated in a pure form and (2) Co(HCO₂)₂ NMR line shape and spin relaxation are strongly perturbed due to the paramagnetic nature of metal ions (Co²⁺). The D₂O (20 mL) was mixed with potassium sulfate (10 g) in a 50 mL glass bottle. The Mg(HCO₂)₂ (~100 mg), placed in a 20 mL vial, was centered in the middle of the 50 mL bottle, ensuring that the sample did not touch the D₂O. The bottle containing the vial was tightly sealed with a cap and placed in a convection oven at 30 °C for a week. The sample was recovered from the vial, without touching the D₂O, and PXRD was used to confirm the structural transformation.

4.2 ²H NMR line shape and relaxation analysis

In an attempt to clarify the role of the confined water molecules in the proton conduction mechanism, a detailed ²H NMR investigation of the fully hydrated Mg(HCO₂)₂ compound was undertaken.

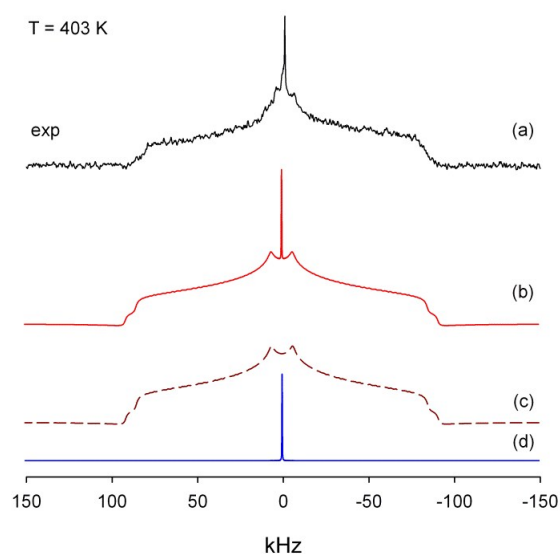


Fig. S10 ^2H NMR spectra line shape for $\text{Mg}(\text{HCO}_2)_2$ at 403 K: (a) experimental; (b) simulated line shape; (c) simulate anisotropic component; (d) simulated isotropic component.

The ^2H NMR spectra show that above 273 K, the pattern does not change considerably: its line shape consists predominantly of a broad anisotropic signal with a large asymmetry parameter ($\eta \sim 0.9$) as well as a relatively weak and narrow isotropic peak in the center of the spectrum. An example of the line shape analysis at 403 K is given in Fig. S10. The broad anisotropic signal shows that most of the confined water molecules are strongly bound onto the $\text{Mg}(\text{HCO}_2)_2$ framework and are only able to perform a well-defined 2-site flipping motion. Above 273 K the pattern indicates a fast exchange limit ($k_{\text{flip}} \gg Q_0 \sim 10^5$ Hz) which is stable until the thermal decomposition of the sample ($T > 423$ K). In this region, the line shape analysis allows for the derivatization of the quadrupolar coupling constant Q_0 and the 2-site 180° -flips geometry. It is found that the coupling tensor ($Q_0 = 245$ kHz, $\eta_0 < 0.01$) is almost axially symmetric and notably larger than in bulk hexagonal ice ($Q_{\text{ice}} = 216$ kHz)^{S10}, which indicates longer hydrogen bonds for the O-D groups. The axial angle in the rotation cone of the 180° -flips is $\theta_{\text{flip}} = 53.2^\circ$, which is only slightly larger than the D-O-D angle in pure water ($2\theta_{\text{D}_2\text{O}} \sim 104.5^\circ$) but considerably lower than the tetrahedral coordination observed in ice.

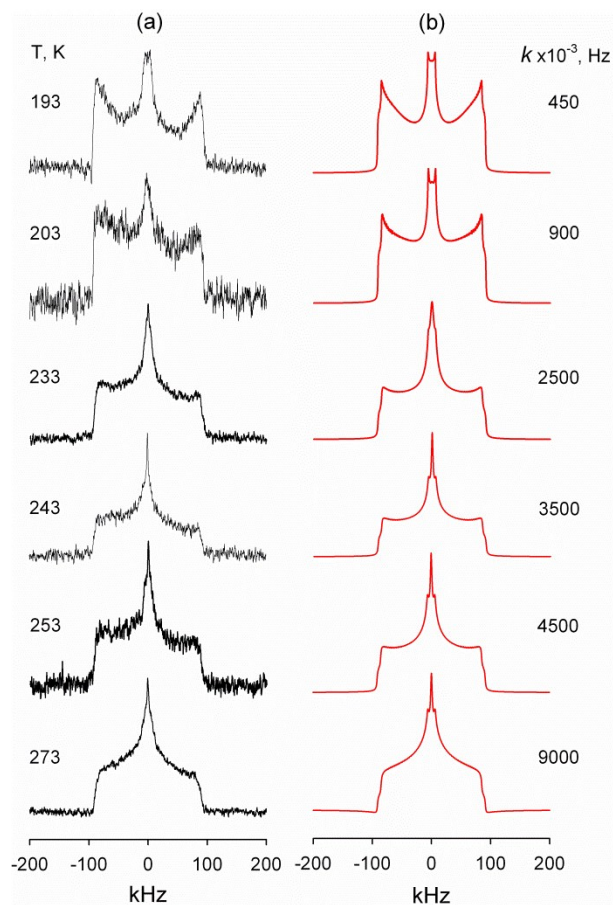


Fig. S11 ^2H NMR spectra line shape for $\text{Mg}(\text{HCO}_2)_2$ as a function of temperatures (a) experimental and (b) simulated.

This is a typical situation for water molecules strongly confined in micropores with weak hydrogen bonding i.e. the deuterons of the coordinated water molecules remain almost free from hydrogen bonding and are mainly restricted by the tight confinement of the framework's pores.^{S11-13} Below 203 K the coupling constant increases up to 255 kHz, which means that additional fast restricted-librational motions of the coordinated water is present. Analysis of the line shapes measured at different solid-echo delays allows for the quantification of the mobile fraction's population. It was found that at 403 it does not exceed 0.2 %. (i.e. $p_{\text{iso}} \sim 0.002$).

In order to estimate the kinetic parameters of the 2-site flips, the line shape evolution was analyzed below 273 K. As shown in Fig. S11, the 2-site flip motion model correlates perfectly with the experimental patterns. The flipping rate constant's, k_{flip} , temperature dependence obeys the

Arrhenius law (see Fig. S12) with an activation barrier of $E_{\text{flip}} = 15.2$ kJ/mol and $k_{\text{flip}0} = 0.7 \times 10^{10}$ Hz (the corresponding correlation time can be computed as $\tau = 1/(2\pi k_{\text{flip}})$, where k_{flip} is given in Hz).

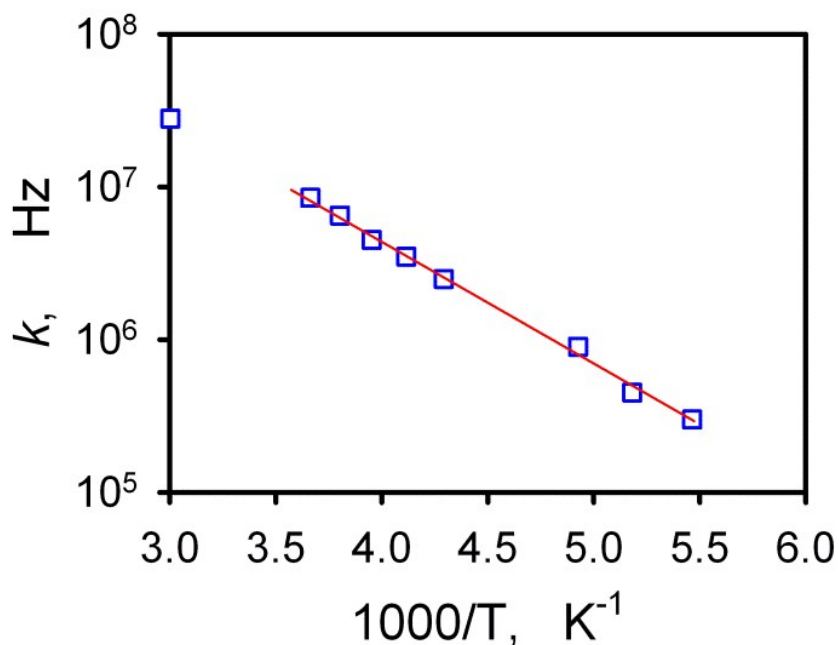


Fig. S 12 The k_{flip} rate constant's temperature dependence in Log scale against the inverse temperature.

The value of the 2-site flip's activation barrier is notably smaller compared to the effective activation barrier of the conductivity, σ . Hence, it must be concluded that the main mode of motion for the O-D groups in the formate is not directly involved in the conduction mechanism and that other possible dynamic modes need to be considered.

Since an isotropic signal, albeit a small fraction, from mobile water molecules is observed, even below 203 K, the dynamics of these water species must be analyzed as well. To do so, the T_1 and T_2 spin relaxation's temperature dependence of both signals was also measured (see Fig. S13).

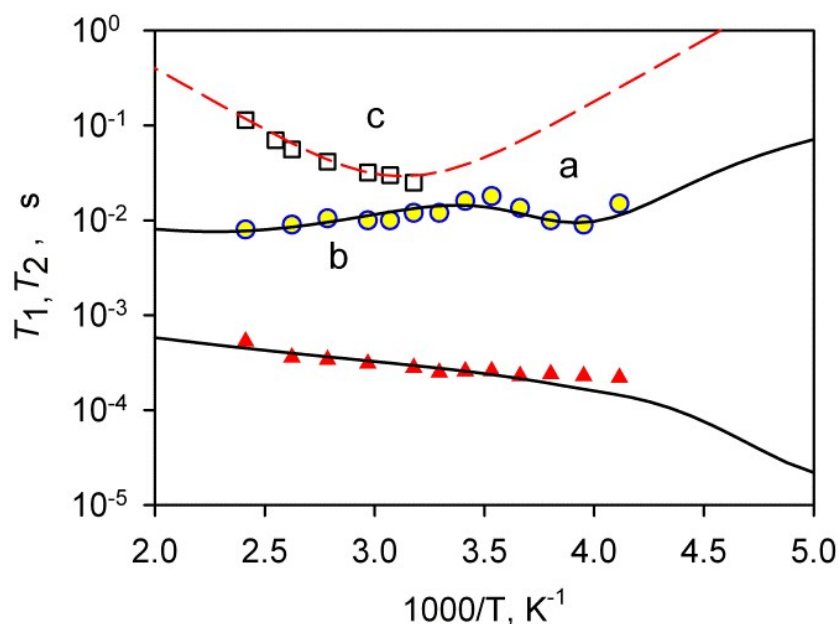


Fig. S13 ^2H NMR spin relaxation times temperature dependences for $\text{Mg}(\text{HCO}_2)_2$. Experimental: (\circ) - anisotropic signal T_1 ; (Δ) - anisotropic signal T_2 ; (\square) - isotropic signal T_1 . Simulation is given by solid and dashed lines.

The T_1 relaxation curve shows the presence of two characteristic minima for the coordinated water species (**a**, **b** in Fig. S13). This means that for the bound water it should have at least 2 modes of motion. One, (marked **a** in Fig. 11), is characterized by a relatively high activation barrier and a surprisingly high pre-exponential factor ($E_{\text{lib}} = 35$ kJ/mol and $k_{\text{lib}0} = 1.5 \times 10^{15}$ Hz). Geometrically these motions are described as restricted angular librations in a cone with $\theta_{\text{lib}}^{\text{anis}} = \pm 15^\circ$. The second mode of motion (marked **b** in Fig. S13) is the 2-site flip, which is described by the same geometry and kinetic parameters as derived from the line shape analysis ($E_{\text{flip}} = 15.2$ kJ/mol and $k_{\text{flip}0} = 0.7 \times 10^{10}$ Hz). The same motion governs the anisotropic T_2 relaxation. The quadrupolar coupling constant derived from the relaxation time analysis yields $Q_0 = 245$ kHz, i.e. a value similar to the one derived from the line shape analysis. This underlines that for coordinated water, no other potentially faster motions are present.

For the mobile species, due to a low population, only 1 minimum at higher temperatures (**c** in Fig. S13) can be unambiguously derived. Since the line shape is represented by an isotropic Lorentzian liquid-like pattern, it is assumed that isotropic reorientation is present. Moreover, its kinetic

parameters are notably different ($E_{\text{iso}} = 25$ kJ/mol and $k_{\text{iso0}} = 1.5 \times 10^{12}$ Hz) while the effective coupling constant for such a simplified model that involves one motion is only $Q_{\text{eff}} = 65$ kHz. This directly indicates to the presence of additional anisotropic motions (like uniaxial rotations) in the mobile species' dynamic pattern.^{S14, S15}

Analysis of the solid-state ^2H NMR data described above demonstrates that the majority of the water in the $\text{Mg}(\text{HCO}_2)_2$ is found coordinated to the metal state, which is fully consistent with the structural analysis. The surrounding molecular environment does not create a strong restriction potential for the coordinated water's local 2-site flips, yet, there is not enough space for efficient hydrogen bonding with the residual "free" water molecules, which is reflected in the very large quadrupolar coupling constant of the water. In addition, this assumption is supported by the second librational mode where the high barrier for this motion is indicative of a sterically very tight confinement formed by the framework pores. As a result, the fraction of mobile water species (D_2O or the charge carrier D_3O^+) does not exceeds 0.2 %, even at elevated temperatures. Thus, in order to further enhance the efficiency of the proton conductivity, an optimal confinement geometry has to be achieved.

5.3 ^2H NMR spectra line shape simulation:

To understand the detailed mechanism of rotations, a detailed fitting analysis of the ^2H NMR spectra line shapes should be performed within an experimentally given temperature range. The in-house FORTRAN simulation routines are based on the general formalism proposed by Abragam⁶ and developed in detail by Spiess^{S16} and others^{S17-S20}.

The fitted spectra are obtained by Fourier transform of the powder-average taken over the polar angles θ and ϕ of the correlation function $G(t, \theta, \phi)$, which governs the time evolution of the transverse ^2H spin magnetization after the solid echo pulse sequence. The correlation function can be computed using the following equation: ^{S18}

$$G(t, \theta, \phi) = \sum_{i,j,k}^{1..N} l_i [\exp (At)]_{ij} [\exp (A\tau)]_{ij} [\exp (A * \tau)]_{jk} P_k \quad (1)$$

where \mathbf{A} is a complex matrix composed as follows:

$$A = \Omega + K, \quad (2)$$

The diagonal matrix Ω is composed of elements ω_i , which describe the frequencies of the exchanging sites, while K corresponds to a kinetic matrix that defines the jump rates.

$$\begin{cases} \Omega_{ii} = i\omega_i - 1/T_2^0 \\ \Omega_{ij} = 0 \end{cases} \quad \text{and} \quad \begin{cases} K_{ii} = -\sum_{j \neq i} k_{ij} \\ K_{ij} = k_{ij}, \end{cases} \quad (3)$$

The $1/T_2^0$ term represents the residual line width which reflects the contributions from homo- and heteronuclear dipolar interactions of the Hamiltonian spin. \mathbf{I} is a vector $(1, 1, \dots, 1)$ with N elements where N is the number of exchange sites. \mathbf{P} is a vector of the equilibrium population of each site $p_{\text{eq}}(i)$ while k_{ij} is the exchange rate between sites i and j . The ^2H NMR frequency at the i -th site $\omega_i(\theta, \varphi)$ is defined as:

$$\omega_i(\theta, \varphi) = \sqrt{\frac{31}{22}} \sum_{a,b=-2}^2 q_{2a} D_{ba}(\Omega^i) D_{a0}(\phi, \theta, 0) q_2 = \left(-\frac{\eta_{OD}}{2}, 0, \sqrt{\frac{3}{2}}, 0, -\frac{\eta_{OD}}{2} \right) Q_{OD}, \quad (4)$$

Here $D_{ba}(\Omega^i)$ are the Wigner rotation matrices^{S16} which define the O-D bond orientation for each site while q_2 is a static interaction tensor (the Wigner matrices are defined here in a way similar to Spiess^{S16}).

If the motion is complex, then the Winger matrix responsible for the transformation of the O-D bond orientation from the system frame of the principal axis, which is fixed, to a given deuteron (the frame with its Z-axis aligned with the O-D bond orientation in this particular case) and to the frame attached to the molecular axis system (i.e. the crystalline axis system), is merely a result of multiple Wigner matrices where each is responsible for a certain rotation, i.e.:

$$D_{ba}(\Omega^i) = \sum_{c,d=-2}^2 D_{bc}(\Omega^1) D_{cd}(\Omega^{\dots}) D_{da}(\Omega^N) \quad (5)$$

In other words, to apply such a jump-model concept to the particular case of protonic species dynamics, a mechanism for these rotations should be specified that includes a set of rotation matrices and the rate matrix that defines the exchange mechanism.

5.4 The anisotropic ^2H NMR spin-lattice relaxation time fitting

Spin relaxation times T_1 and T_2 are generally anisotropic and depend on the observation angles θ and φ in the powder pattern. They are given by the usual formulae: ^{S16}

$$\frac{1}{T_1} = \frac{3}{4}\pi^2 Q_0^2 (J_1(\omega_0) + 4J_2(2\omega_0)) \quad (6)$$

$$\frac{1}{T_2} = \frac{3}{8}\pi^2 Q_0^2 (3J_1(0) + 5J_1(\omega_0) + 2J_2(2\omega_0)) \quad (7)$$

where the spectral density function $J_m(\omega)$ for the chosen model of molecule motion is defined by the expression:

$$J_m(\omega) = 2 \sum_{a,b=-2}^2 D_{m,a}(\Omega_L) * D_{m,b}(\Omega_L) \sum_{l,k,n=1}^N D_{3,a}^l(\Omega_l) * D_{3,b}^k(\Omega_k) p_{eq}(l) V_{l,n} \left(\frac{-\lambda_n}{\lambda_n^2 + \omega^2} \right) V_{n,k}^{-1} \quad (8)$$

Here Ω_L represents the observation angles θ and φ which connect the molecular frame with the laboratory frame, Ω_k is the Euler angles which connect the molecular frame with the k -th distinct position of the C - D bond within the assumed geometry of the jump model, $V_{l,n}$ is a matrix composed of Eigenvectors in a kinetic matrix K , where λ_n are its Eigenvalues, and N is the number of distinct jump-sites.

If one or multiple isotropic motions are present, then the corresponding correlation function is no longer dependent on the polar angles and the resulting function is simply a tensor multiplication of correlation functions for distinct motional modes.

5.5 ^2H NMR Sample Preparation.

The NMR samples preparation is as follows: the crystal powder was transferred into a special glass cell with a vacuum grade valve and small dead volume under an argon atmosphere. The cell was subsequently connected to the vacuum line and kept under liquid nitrogen conditions. Then the cell was pumped for several seconds to get rid of atmospheric oxygen. This flushing was repeated four times. Finally, the part of the cell containing the sample was sealed by flame under liquid nitrogen conditions.

5.6 NMR Measurements

^2H NMR experiments were performed at 61.424 MHz on a Bruker Avance-400 spectrometer using a high power probe with a 5 mm horizontal solenoid coil. All ^2H NMR spectra were obtained by Fourier transformation of the quadrature-detected phase-cycled quadrupole echo arising in the pulse sequence $(90_x - \tau_1 - 90_y - \tau_2 - \text{acquisition} - t)$, where $\tau_1 = 20 \mu\text{s}$, $\tau_2 = 21 \mu\text{s}$, and t is a repetition time of the sequence during the accumulation of the NMR signal. The duration of the $\pi/2$ pulse was 1.8 - 2.1 μs . Spectra of hydrated TPA were typically obtained after 100 - 1000 scans with repetition times ranging from 1 to 10 seconds, depending on the sample conditions.

Inversion-recovery experiments to derive spin-lattice relaxation times (T_1) were carried out using the pulse sequence $(180_x - \tau_v - 90_{\pm x} - \tau_1 - 90_y - \tau_2 - \text{acquisition} - t)$, where t_v was a variable delay between the 180°_x inverting pulse (as in standard inversion recovery pulse sequence) and the quadrupole echo sequence.

To capture all dynamical features of the system, the measurements were performed over a broad temperature range from 103 K to 413 K. The temperature of the samples was controlled with a variable-temperature unit BVT-3000 with a precision of ± 1 K. The sample was allowed to

equilibrate at least 15 min at a given temperature before the NMR signal was acquired.

References

- S1. H. Kim, D. G. Samsonenko, M. Yoon, J. W. Yoon, Y. K. Hwang, J.-S. Jang and K. Kim, *Chem. Commun*, 2008, 4697-4699.
- S2. A. J. Arvai and C. Nielsen, ADSC Quantum-210 ADX Program, Area Detector System Corporation; Poway, CA, USA, 1983.
- S3. Z. Otwinowski, W. Minor, in *Methods in Enzymology*, ed. C. W. Carter, Jr. and R. M. Sweet, Academic Press, New York, 1997, vol. 276, part A, pp. 307.
- S4. SHELX program: G. W. Sheldrick, *Acta Crystallogr.* 2015, **C71**, 3.
- S5. Fit2D program: A. P. Hammersley, *J. Applied Cryst.*, 2016, **49**, 646–652.
- S6. Conograph program: A. Esmaili, T. Kamiyama, R. Oishi-Tomiyasu, *J. Appl. Cryst.*, 2017, **50**, 651.
- S7. K. Osaki, Y. Nakai, T. Watanabe, *J. Phys. Soc. Jpn.*, 1964, **19**, 717-723.
- S8. C. R. Groom, I. J. Bruno, M. P. Lightfoot and S. C. Ward, *Acta Cryst.*, 2016, **B72**, 171-179.
- S9. A. Kaufman, C. Afshar, M. Rossi, D. E. Zacharias, and J. P. Glusker, *Struct. Chem.*, 1993, **4**, 191-198.
- S10. R. J. Wittebort, M. G. Usha, D. J. Ruben, D. E. Wemmer, A. Pines, *J. Am. Chem. Soc.*, 1988, **110**, 5668-5671.
- S11. A. E. Khudozhitkov, P. Stange, B. Golub, D. Paschek, A. G. Stepanov, D. I. Kolokolov, R. Ludwig, *Angew. Chem., Int. Ed.*, 2017, **56**, 14310-14314.
- S12. T. Chiba, *J. Chem. Phys.* 1964, **41**, 1352-1358.
- S13. R. Blinc, D. Hadzi, *Nature* 1966, **212**, 1307-1309.
- S14. A. E. Khudozhitkov, P. Stange, A.-M. Bansa, V. Overbeck, V. Appelhagen, A. G. Stepanov, D. I. Kolokolov, D. Paschek, R. Ludwig, *Chem. Comm.* 2018, **54**, 3098-3101.
- S15. A. Abragam, *The Principles of Nuclear Magnetism*; Oxford University Press: Oxford, UK, 1961.
- S16. H. W. Spiess, Rotation of Molecules and Nuclear Spin Relaxation. In *NMR Basic Principles and Progress*, Diehl, P.; Fluck, E.; Kosfeld, R., Eds. Springer-Verlag: New York, 1978; Vol.

15, p 55 –214.

S17. R. J. Wittebort, A. Szabo, *J. Chem. Phys.* 1978, **69**, 1722.

S18. R. J. Wittebort, E. T. Olejniczak, R. G. Griffin, *J. Chem. Phys.* 1987, **86**, 5411-5420.

S19. G. Lipari, A. Szabo, *Biophys. J.* 1980, **30**, 489-506.

S20. L. J. Schwartz, E. Meirovitch, J. A. Ripmeester, J. H. Freed, *J. Phys. Chem.* 1983, **87**, 4453-4467.